

Evolution of multimodal fission with energy in ^{238}Np populated by $^6\text{Li} + ^{232}\text{Th}$

Tathagata Banerjee ^{1,2,*}, E. M. Kozulin ¹, G. N. Knyazheva ¹, A. A. Bogachev ¹, I. M. Itkis ¹, E. Vardaci ^{3,2},
A. Di Nitto ^{3,2}, M. Ashaduzzaman ³, P. A. Setaro ³, and G. Alifano ³

¹Flerov Laboratory of Nuclear Reactions, Joint Institute for Nuclear Research, Dubna 141980, Russia

²Istituto Nazionale di Fisica Nucleare, Sezione di Napoli, 80126 Napoli, Italy

³Dipartimento di Fisica “E. Pancini”, Università degli Studi di Napoli “Federico II”, 80126 Napoli, Italy



(Received 2 May 2023; accepted 7 November 2023; published 4 December 2023)

Background: Nuclear fission is influenced by shell effects. Fission modes are a strong signature of the compound nucleus formation in heavy ion induced reactions. The evolution of the relative strengths of the fission modes with excitation energy is a matter of intense interest.

Purpose: We investigate the signatures of fission modes in ^{238}Np populated by the $^6\text{Li} + ^{232}\text{Th}$ reaction through the mass–total kinetic energy distribution.

Method: The mass–total kinetic energy distributions of fission fragments of the reaction $^6\text{Li} + ^{232}\text{Th}$ are measured at four laboratory energies, $E_{\text{lab}} = 28.5, 40, 45,$ and 62.5 MeV. Mass–total kinetic energy distributions of $^6\text{Li} + ^{232}\text{Th}$ are described by the multimodal random neck rupture model.

Results: Channel probabilities of different fission modes are obtained through a two-dimensional fitting procedure. The contribution of the standard 1 (S1) mode is found to become $\approx 2\%$ at $E_{\text{lab}} = 40$ MeV. The heavy fragments of S1 and standard 2 (S2) modes are found to be associated with $Z \approx 52$ and $Z \approx 55$ shells, respectively. The slope of the asymmetric to symmetric fission yields ratio with the excitation energy of $^6\text{Li} + ^{232}\text{Th}$ is found to be similar to that of $^{18}\text{O} + ^{208}\text{Pb}$ (previously reported).

Conclusions: The analysis of mass–total kinetic energy distribution data reveals the presence of fission modes in $^6\text{Li} + ^{232}\text{Th}$. The average kinetic energy release in fission obtained from Viola systematic matches well with the one of the S2 mode. The liquid-drop-like broad symmetric (SL) mode is found to peak at a lower energy than predicted by Viola systematic. This is associated with the decrease of the total kinetic energy in the asymmetric fission mode due to the fading out of shell effects with increasing excitation energy.

DOI: [10.1103/PhysRevC.108.064601](https://doi.org/10.1103/PhysRevC.108.064601)

I. INTRODUCTION

A compound nucleus (CN), formed by the complete fusion (CF) of a projectile and a target nucleus may decay by various paths. The CN can fission or cool off by emitting γ rays, neutrons, or light charged particles to yield an evaporation residue. If heavy enough, the CN can fission in different channels/modes (i.e. symmetric and/or asymmetric). Brosa *et al.* [1] developed the multimodal random neck rupture (MM-RNR) model that can deconvolute the mass distribution (MD) and/or mass–total kinetic energy distribution (M-TKED) into different fission modes, one symmetric: “superlong” (SL) and/or “supershort” (SS) mode; and four asymmetric modes: “Standard 1” (S1), “Standard 2” (S2), “Standard 3” (S3), and superasymmetric (SA) mode. A detailed description of different fission modes can be found elsewhere [1,2]. The analysis of the multimodal fission at high excitation energies (E^*) using M-TKED in heavy ion induced reactions is rather scarce.

Beside the CF where all the charge of the projectile is captured by the target, associated with the full momentum

transfer (FMT) of the projectile, there are fusion processes following breakup of the projectile: (i) incomplete fusion (ICF) and (ii) sequential complete fusion (SCF). In ICF, one of the broken fragments of the projectile is captured by the target [3–5], whereas, in SCF, all broken fragments of the projectile are sequentially absorbed by the target [6].

There can be fission induced by the direct transfer of a few nucleons to the target from the projectile, named transfer fission (TF), in cases of reactions with actinide targets. Though it is difficult to distinguish between breakup and TF due to their similar energetics and final outcome (final residual nucleus), there is a difference between these two processes. The breakup process proceeds via the Coulomb or nuclear excitation of the projectile nucleus in the field of the target while the transfer process depends on the detailed structure of participating nuclei [7–9].

Nuclei which have binding energies (BE) less than ≈ 3 MeV are classified as weakly bound nuclei (WBN). Examples of such nuclei are ^6Li and ^7Li [10–14]. ^6Li has a cluster structure and has no bound excited state. It breaks up into $\alpha + d$ at 1.48 MeV (α separation energy $S_\alpha = 1.48$ MeV). In reactions involving a WBN as the projectile and an actinide nucleus as the target, fission fragments (FF) may originate from a breakup/transfer induced fission which does not comply with

*he.tatha@gmail.com

FMT. Consequently the fission fragment folding angle distribution includes events that do not correspond to FMT [9,15–23]. In order to correctly identify the fission modes from the CN those events should be identified and removed.

The main goal of this work is searching for the fission modes in the reaction ${}^6\text{Li} + {}^{232}\text{Th}$ and studying their evolution with increasing excitation energy.

The M-TKED of fission fragments of the reaction ${}^6\text{Li} + {}^{232}\text{Th}$ was measured at four laboratory energies, $E_{\text{lab}} = 28.5, 40, 45, \text{ and } 62.5$ MeV. The experimental details are described in Sec. II. The M-TKEDs are presented in Sec. III. The possible presence of multimodal fission is investigated using the MM-RNR model [1] in Sec. IV followed by conclusions in Sec. V.

II. EXPERIMENTAL DETAILS

This paper reports the reanalysis of data which was originally published earlier [15]. Measurements were carried out using ${}^6\text{Li}$ beams from the U400 cyclotron accelerator of the Flerov Laboratory of Nuclear Reactions at the projectile energies $E_{\text{lab}} = 28.5, 40, 45$ and 62.5 MeV. A $190 \mu\text{g}/\text{cm}^2$ thick ${}^{232}\text{Th}$ layer, evaporated onto a $35 \mu\text{g}/\text{cm}^2$ carbon backing, was used as the target. The double-arm time-of-flight spectrometer CORSET [24] was used for the registration of fission fragments that were subsequently mass identified by the method of kinematics coincidences. Each arm of the spectrometer consisted of start and stop detectors composed of microchannel plates, which were used for registering the secondary electron emission produced in the interaction of fission fragments with entrance foils of the detectors. Each start detector was $2.5 \times 3.5 \text{ cm}^2$ in size and was equipped with an electrostatic mirror. The stop detectors, $6 \times 9 \text{ cm}^2$ in size, were position sensitive (x, y sensitive).

The start detectors were positioned at a distance of 3.8 cm from the target. The minimal flight path (the distance between the start and the stop detectors) was 16.2 cm . The angular resolution of the spectrometer was $\approx 0.1^\circ$. Its mass resolution was tested with the use of a ${}^{252}\text{Cf}$ spontaneous fission source. From the measured M-TKED of fission fragments the mass resolution of the spectrometer was estimated to be at the level of $3\text{--}5 \text{ u}$. For M-TKED measurements, in this particular case, the spectrometer arms were positioned symmetrically at the angles of $\pm 85^\circ$ with respect to the beam axis, and the acceptances of each arm were 24.6° and 19.2° in and out of the reaction plane, respectively.

III. M-TKED OF BINARY FRAGMENTS OF ${}^6\text{Li} + {}^{232}\text{Th}$

The experimental data were processed assuming standard two-body kinematics. The analysis was carried out following a well established method [2,15,24].

The separation angle between the velocity vectors of the coincident fission fragment pairs serves as an indicator of the linear momentum transferred from the incident projectile to the struck nucleus [25–27]. The CNF fragments after fusion having full momentum transfer are emitted with a unique separation angle ($\theta_{\text{fold}}^{\text{CNF}}$) in laboratory frame of reference defined by the momenta of the projectile and the primary fragments.

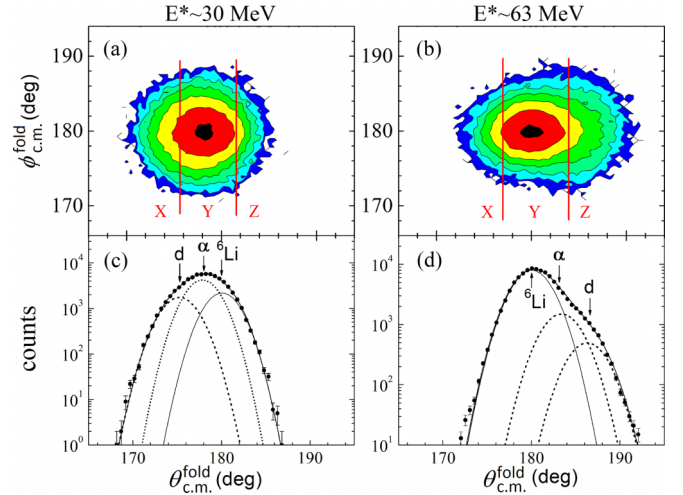


FIG. 1. The 2D plots of FF folding angle distribution in the reaction plane ($\theta_{\text{c.m.}}^{\text{fold}}$) versus out of that plane $\phi_{\text{c.m.}}^{\text{fold}}$ for two E^* s 30 MeV and 63 MeV of ${}^6\text{Li} + {}^{232}\text{Th}$ are shown in panels (a) and (b). Regions of small (X), medium (Y) and large (Z) angles are shown. The projections of the whole data in panels (a) and (b) are shown in panels (c) and (d), respectively (see text for details). Adapted from Ref. [15].

The $\theta_{\text{fold}}^{\text{CNF}}$ for ${}^6\text{Li} + {}^{232}\text{Th}$ calculated from the kinematics which assumes symmetric mass division and the total kinetic energy release in fission predicted by Viola systematics [28] is 173° at $E_{\text{lab}} = 28.5 \text{ MeV}$. Thus for fusion-fission, the angular correlation centroid angle in the laboratory frame should be centered around 173° . In reactions with actinide targets, transfer-induced fission (TF) also occurs, but at different folding angles. In few-nucleon transfer reactions, little momentum is imparted to the fissioning nucleus, leading to separation angles near $\theta_{\text{fold}}^{\text{TF}} \approx 180^\circ$ in the laboratory frame.

On the other hand, in the center-of-mass (c.m.) frame, for a true binary process with FMT, the FF folding angle distribution should be centered around $\theta_{\text{c.m.}}^{\text{CNF}} = 180^\circ$. In TF, a beamlike particle is ejected with much more momentum than neutrons evaporated by the CN that are isotropic and not focused as the nonfused part of the projectile. Since transfer reactions occur at a limited range of angles around the grazing angle (rather than isotropically), the FF folding angle distribution would also be asymmetric, having “shoulders.”

The two-dimensional (2D) plots of FF folding angle distribution in the reaction plane ($\theta_{\text{c.m.}}^{\text{fold}}$) versus out of that plane $\phi_{\text{c.m.}}^{\text{fold}}$ for two E^* s, 30 and 63 MeV (adapted from Ref. [15]) of ${}^6\text{Li} + {}^{232}\text{Th}$ are shown in panels (a) and (b) in Fig. 1. Regions of small (X), medium (Y) and large (Z) angles are shown. The projection in the $\theta_{\text{c.m.}}$ shows the convolution of three distributions corresponding to ${}^6\text{Li}$, α , and d [shown in panels (c) and (d)].

At $E^* \approx 30 \text{ MeV}$, the projectilelike nucleus recoils to backward angles associated with a grazing angle of $\approx 180^\circ$ in the laboratory frame, then the folding angles between the fragments are lower than the compound nuclear fission (CNF) ones [i.e., the transfer fission events' $\theta_{\text{c.m.}}^{\text{TF}} < 180^\circ$; see panel (c) of Fig. 1]. On the other hand, at $E^* \approx 63 \text{ MeV}$, the

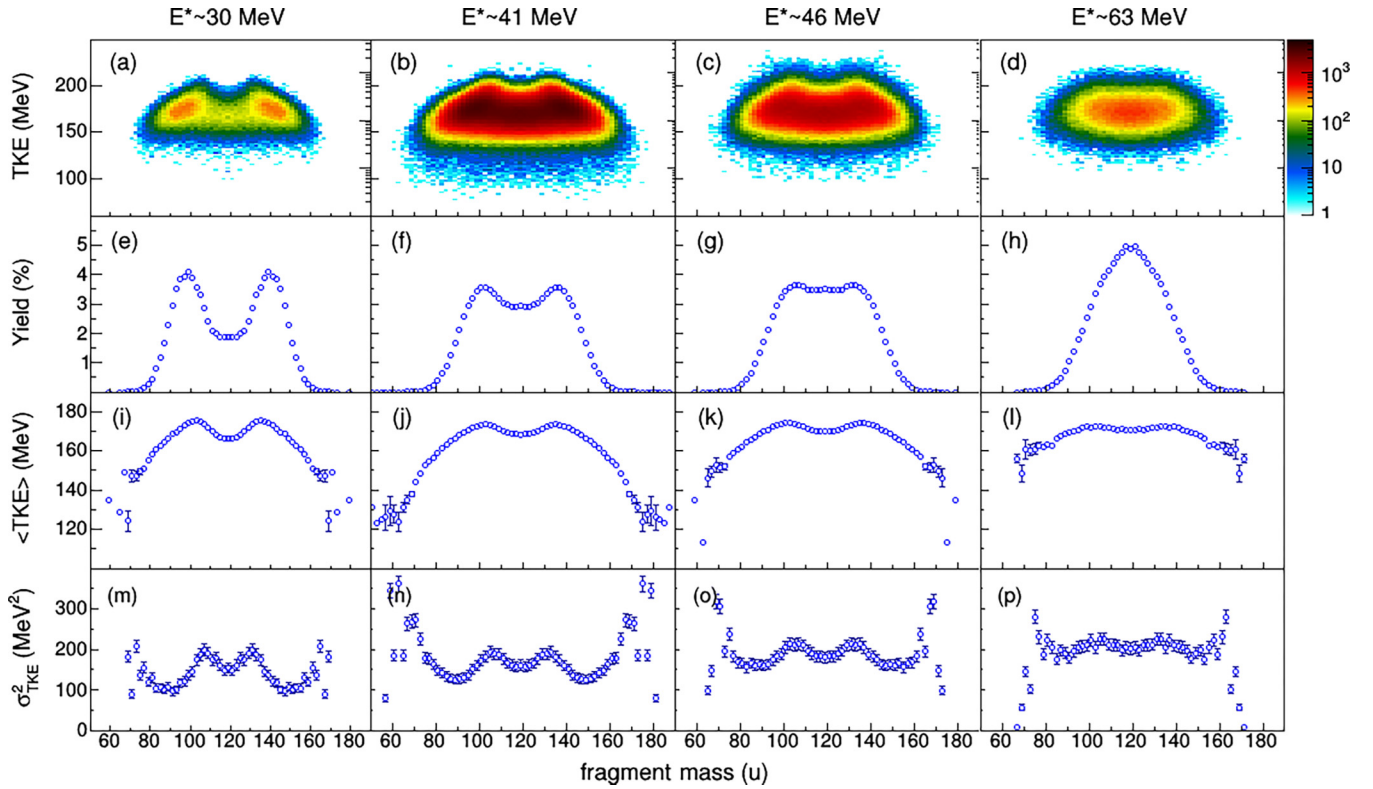


FIG. 2. M-TKEDs of the binary fragments of the reaction ${}^6\text{Li} + {}^{232}\text{Th}$ at $E^* = 30, 41, 46,$ and 63 MeV are shown in panels (a)–(d). Corresponding gated MDs, $\langle\text{TKE}\rangle$, and the variances of the TKE (σ_{TKE}^2) are shown in panels (e)–(h), (i)–(l), and (m)–(p), respectively.

projectilelike nucleus recoils in the forward direction (grazing angle $<90^\circ$ in the laboratory frame) and the folding angles between the fragments are larger than the CNF ones [i.e., the transfer fission events' $\theta_{\text{c.m.}}^{TF} > 180^\circ$; see panel (d) of Fig. 1]. The deflection angle and consequently the position of the peak of α and d in the projection spectra on the $\theta_{\text{c.m.}}^{\text{fold}}$ axis would depend on the mass of the particle. At intermediate energies, the FF folding angle distribution would be intermediate between those two extremes, having contribution from the transfer-induced fission events at both forward and backward angles [15].

The binary products of the reaction with FMT were selected by putting a gate window of 3.5° centered at 180° in the FF folding angle distribution. This excludes the asymmetric mass distribution of region Z at higher energy and of region X at lower energy. The M-TKED of the primary binary fragments obtained in this way in the reaction under investigation at CN excitation energies of $\approx 30, \approx 41, \approx 46,$ and ≈ 63 MeV, mass distribution (MD) of fission fragments, average total kinetic energy ($\langle\text{TKE}\rangle$), and the variance of the TKE distribution (σ_{TKE}^2) as functions of fragment mass are shown in Fig. 2. The MDs are normalized to 200% considering the fact that the CN leads to two fission fragments. It is clear from Fig. 2 that the MDs are not single Gaussian in nature. A gradual transition from asymmetric to symmetric structure can be seen with increasing E^* . Moreover, the multiple humps in the MDs, $\langle\text{TKE}\rangle$, and σ_{TKE}^2 call for a multimodal analysis [35,36].

IV. SEARCH FOR THE MULTIMODAL FISSION IN ${}^6\text{Li} + {}^{232}\text{Th}$

A. Calculation of the mass width of the SL mode

The search for the fission modes consists in finding the mass numbers that contribute to the peaks and valleys of the mass distribution and how their relative strength changes with the excitation energy. This search is usually done empirically and considering each single contribution, shaped according to a Gaussian curve in the lack of any other information. Systematics are also used as well as expectations of the liquid drop (LD) model. This same ansatz is also extended to the TKE distribution. In this paper, a 2D method is used instead. We will try to fit the mass and TKE distribution simultaneously in the same fit, contrarily to what is usually done.

Figure 3 deals with the extraction of the superlong (SL) mass widths (σ_m). To gain reliability of the extraction of these for ${}^6\text{Li} + {}^{232}\text{Th}$, first we adopted a procedure to match some observables for the ${}^6\text{Li} + {}^{208}\text{Pb}$ reaction having no quasifission and no transfer induced fission. By adopting the same procedure and the same code, we extracted several quantities, among which are the SL mass widths. These quantities, then, would be assumed as the fixed parameters in the 2D fitting of the M-TKE distributions.

As the SL mode is due to the macroscopic liquid drop (LD) part of the potential energy, and is not affected by shell corrections, its mass widths were obtained from the LD model (LDM) calculation first, before fitting the 2D M-TKED.

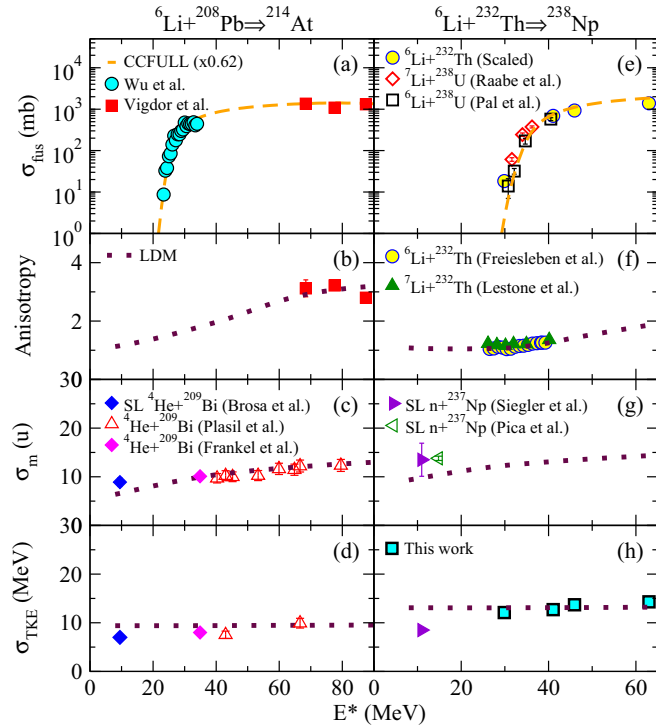


FIG. 3. Comparison of measured fusion cross sections of ${}^6\text{Li} + {}^{208}\text{Pb}$ [40,41] and ${}^6\text{Li} + {}^{232}\text{Th}$ [15,30] with the CCFULL predictions (dashed orange line) are shown in panels (a) and (e), respectively. The CCFULL prediction of ${}^6\text{Li} + {}^{208}\text{Pb}$ is scaled by 0.62. The total fission cross section of Ref. [30] is scaled by the factors ($\sigma_{\text{fusion}}/\sigma_{\text{fiss}}$) reported in Ref. [15] to obtain the fusion cross section of ${}^6\text{Li} + {}^{232}\text{Th}$. The data of ${}^{6,7}\text{Li} + {}^{238}\text{U}$ [16,21] are also shown for the sake of comparison. The FF angular anisotropy, mass widths, and TKE widths of ${}^6\text{Li} + {}^{208}\text{Pb}$ and ${}^6\text{Li} + {}^{232}\text{Th}$ predicted by LDM are represented by dotted maroon lines. Measured anisotropies of ${}^6\text{Li} + {}^{208}\text{Pb}$, ${}^{232}\text{Th}$ are taken from Refs. [30,49]. The widths of mass and TKE of the reaction ${}^4\text{He} + {}^{209}\text{Bi}$ are taken from Refs. [1,45–48]. The widths of mass and TKE of $n + {}^{237}\text{Np}$ are taken from [50,51] (see text).

The mass widths of the SL mode were calculated using the following equation [37]:

$$\sigma_m^2 = \frac{M_{\text{CN}}^2 T_{\text{saddle}}}{16} \left[\left(\frac{d^2V}{d\eta^2} \right)_{\eta=0} \right]^{-1} + \frac{\partial \sigma_m^2}{\partial \langle \ell^2 \rangle} (\ell^2), \quad (1)$$

where $(\frac{d^2V}{d\eta^2})_{\eta=0}$ is the stiffness of a nucleus for symmetric mass division ($\eta = 0$) and at zero angular momentum [37]. An example of the application of Eq. (1) is in Fig. 3(c). Though the sensitivity of the variance to the angular momentum is weak, it was still considered, and the term $\frac{\partial \sigma_m^2}{\partial \langle \ell^2 \rangle}$ was taken from the theoretical calculation of Ref. [38]. T_{saddle} is the nuclear temperature at the saddle point. The methodology of calculating T_{saddle} can be found elsewhere [2,39].

To check the reliability of the calculated mass widths, the reaction ${}^6\text{Li} + {}^{208}\text{Pb}$, having no transfer induced fission or quasifission, was taken as a reference. To estimate the

mean square angular momentum $\langle \ell^2 \rangle$ for the different excitation energies we used the measured fusion cross sections of ${}^6\text{Li} + {}^{208}\text{Pb}$ [40,41] and ${}^6\text{Li} + {}^{232}\text{Th}$ [15,30] and the CCFULL code [42] [dashed orange line in panels (a) and (e), respectively, of Fig. 3]. The CCFULL prediction of ${}^6\text{Li} + {}^{208}\text{Pb}$ had to be scaled by 0.62 to match the data. The total fission cross sections at four energies of ${}^6\text{Li} + {}^{232}\text{Th}$ from Ref. [30] had to be scaled by the factors ($\sigma_{\text{fusion}}/\sigma_{\text{fiss}}$) reported in Ref. [15] to obtain the fusion cross section of the same reaction. It can be seen from Fig. 3(e) that the scaled points of ${}^6\text{Li} + {}^{232}\text{Th}$ are nicely matching with the fusion data of ${}^{6,7}\text{Li} + {}^{238}\text{U}$ [16,21]. This provided the reliability of the calculation of the SL mass width.

The Woods-Saxon parametrization of the Akyüz-Winther potential [43] was used as initial values for the three ingredients of the nuclear potential used in CCFULL, viz., the depth V_0 , the radius r_0 and the diffuseness parameter a . As CCFULL cannot handle shallow potentials, a deeper potential was used. In the present scenario $V_0 = 128.0$ MeV, which is in agreement with the value used previously for the ${}^6\text{Li} + {}^{159}\text{Tb}$ reaction in Ref. [44]. The parameters r_0 and a were slightly modified to reproduce the fusion data of ${}^6\text{Li} + {}^{232}\text{Th}$ properly. The values of r_0 and a used were 1.118 fm and 0.621 fm, respectively, instead of 1.177 fm and 0.620 fm obtained from the Woods-Saxon parametrization of the Akyüz-Winther potential. Rotational coupling to the target ${}^{232}\text{Th}$ (with $\beta_2 = 0.248$ and $\beta_4 = 0.108$) was taken into account. Thus, the mean square angular momenta $\langle \ell^2 \rangle$ were obtained from the matched cross sections using CCFULL [42] for both the reactions ${}^6\text{Li} + {}^{208}\text{Pb}$ and ${}^6\text{Li} + {}^{232}\text{Th}$.

The LDM predictions for FF angular anisotropy, mass width, and TKE width [dotted maroon line in Figs. 3(b)–3(d)] for the reaction ${}^6\text{Li} + {}^{208}\text{Pb}$ using a level density parameter (little a) $a = M_{\text{CN}}/8.5$ could reproduce the measured data of the same reaction (and of ${}^4\text{He} + {}^{209}\text{Bi}$ [1,45–48], which populates a nearby CN ${}^{213}\text{At}$). This supports the choice of the value of the parameter a .

Next, the FF angular anisotropy, mass width, and TKE width of the reaction ${}^6\text{Li} + {}^{232}\text{Th}$ were calculated with the same level density parameter value $a = M_{\text{CN}}/8.5$ [dotted maroon line in Figs. 3(b)–3(h)]. The calculation reproduces the measured FF angular anisotropy data for ${}^6\text{Li} + {}^{232}\text{Th}$ [30,49] and measured SL mass widths (obtained after fitting the measured MD) and TKE widths of $n + {}^{237}\text{Np}$ [50,51], which populates the same CN ${}^{238}\text{Np}$. The comparison with two σ_m measured in the $n + {}^{237}\text{Np}$ reaction, referring to the fission decay of ${}^{238}\text{Np}$ compound nucleus, provides an indication on the reliability of the extracted values. The SL mass widths of ${}^6\text{Li} + {}^{232}\text{Th}$ were kept fixed at these calculated values during the 2D fitting of M-TKED. The reaction parameters for ${}^6\text{Li} + {}^{232}\text{Th}$ are presented in Table I.

B. 2D fitting of M-TKEDs of binary fragments of ${}^6\text{Li} + {}^{232}\text{Th}$

It is important to fit both the MD and TKED simultaneously [52] to achieve a more accurate estimate of the location in mass and energy of the fission modes as sometimes fitting MD and TKED separately leads to results which do not match. The 2D M-TKEDs were analyzed within the framework of

TABLE I. The reaction parameters for ${}^6\text{Li} + {}^{232}\text{Th}$ are presented. The center-of-mass energy ($E_{\text{c.m.}}$) is the mean energy in the middle of the target. V_B is the calculated capture barrier of Bass [29]. The critical angular momentum for fusion ($\ell_{\text{crit}}^{\text{fus}}$) derived from the experimental fusion cross sections [15,30] assuming the sharp cutoff approximation, the maximum angular momentum corresponding to the grazing angle (at the distance of closest approach) ($\ell_{\text{max}}^{\text{graz}}$) [31], and the angular momentum for which the fission barrier goes to zero ($\ell_{B_f=0}$) [32] are mentioned. $Z_P Z_T$, χ_{CN} , χ_{eff} , χ_m , η , α_{BG} are the charge product, compound nuclear fissility, effective fissility, mean fissility [33], entrance channel mass asymmetry, and Businaro-Gallone critical mass asymmetry [34], respectively. The experimental TKE widths (σ_e^{exp}) are also presented.

E_{lab} (MeV)	$E_{\text{c.m.}}$ (MeV)	$E_{\text{c.m.}}/V_B$	E^* (MeV)	$\ell_{\text{crit}}^{\text{fus}}$ (\hbar)	$\ell_{\text{max}}^{\text{graz}}$ (\hbar)	$\ell_{B_f=0}$ (\hbar)	$Z_P Z_T$	χ_{CN}	χ_{eff}	χ_m	η	α_{BG}	σ_e^{exp} (MeV)
28.5	27.8	0.84	29.9	2	0								12.1 ± 0.08
40.0	39.0	1.18	41.1	16	15	72	276	0.804	0.263	0.398	0.950	0.889	12.7 ± 0.02
45.0	43.9	1.33	46.0	19	20								13.7 ± 0.04
62.5	60.9	1.84	63.0	28	33								14.3 ± 0.07

MM-RNR model [1] using the following function:

$$Y(M, \text{TKE}) = \sum_i \frac{w_i}{\sqrt{2\pi}\sigma_i^2} \exp\left(-\frac{(M - \langle M_i \rangle)^2}{2\sigma_i^2}\right) \left(\frac{200}{\text{TKE}}\right)^2 \times \exp\left(\frac{2(d_{\text{max},i} - d_{\text{min},i})}{d_{\text{dec},i}} - \frac{L_i}{d_{\text{dec},i}} - \frac{(d_{\text{max},i} - d_{\text{min},i})^2}{L_i d_{\text{dec},i}}\right), \quad (2)$$

where

$$L_i = d - d_{\text{min},i} = \frac{Z_L Z_H e^2}{\text{TKE}} - d_{\text{min},i} \approx \frac{\langle M_i \rangle (M_{\text{CN}} - \langle M_i \rangle) \left(\frac{Z_{\text{CN}}}{M_{\text{CN}}}\right)^2 e^2}{\text{TKE}} - d_{\text{min},i}, \quad (3)$$

where w_i and σ_i are the weights and the widths of the Gaussians centered at $\langle M_i \rangle$'s, corresponding to different fission modes. M_{CN} is the mass of the fissioning nucleus. The mean mass of the SL mode and the width of the S1 mode were fixed at $\frac{M_{\text{CN}}}{2}$ and 3.0 u, respectively, in order to avoid nonphysical convergence.

The maximum TKE is governed by a cutoff due to the Q value of the reaction. The TKED is better represented by a skewed Gaussian distribution. The parameter $d_{\text{max},i}$ gives the distance between the fragment charges at the maximum of the yield distribution, whereas $d_{\text{min},i}$ is the minimum distance between the fragment charge centers corresponding to an upper limit of the TKE, and the parameter $d_{\text{dec},i}$ describes the exponential decrease of the yield with increasing d (the approximated distance between the two fragment charge centers). Z_L (M_L), Z_H (M_H), and Z_{CN} (M_{CN}) are the charges (masses) of the light and heavy fragments and CN, respectively. As charges are not measured, one can assume an unchanged charge density, i.e., $Z_L/M_L \approx Z_H/M_H \approx Z_{\text{CN}}/M_{\text{CN}}$ [2].

One fission mode in 2D distribution requires six parameters (w_i , σ_i , $\langle M_i \rangle$'s, $d_{\text{max},i}$, $d_{\text{min},i}$, and $d_{\text{dec},i}$) to be fitted. The fits to the data of $E^* = 30, 41, 46,$ and 63 MeV are shown in Figs. 4–7, respectively. Three modes (SL, S1, S2) were necessary to fit the data with good accuracy. The SL mode is presented by continuous black lines whereas S1, S2 modes

are shown by dashed green and blue lines. The continuous red lines represent the total fits.

Due to very low yields of very asymmetric (light fragment mass ≈ 84) and supersymmetric (light fragment mass ≈ 70) regions [53], and to avoid nonphysical convergence, the S3 and SA modes could not be accommodated. This explains the deviation of the fits from the measured data at higher fragment mass number. The reduced χ^2 ($\tilde{\chi}^2$) obtained for each fit is also mentioned in Table II. Moreover, the M-TKEDs at 46 and 63 MeV excitation energies could be fitted only with two (SL and S2) modes. The contribution of the S1 mode has already become little ($\approx 2\%$) at the 41 MeV excitation. Thus the component required, other than that representing the SL mode, to fit the M-TKED in the case of the last two high energies, may represent a superposition of the multiple asymmetric modes (S1, S2, etc.), leading to an increase in the $\langle \text{TKE} \rangle$.

The $\langle \text{TKE} \rangle$'s of SL, S1, and S2 modes ($\approx 166.4, \approx 191,$ and ≈ 176.6 MeV, respectively) are in agreement with the values obtained from the multimodal analysis of the SF of nearby nuclei ${}^{236}\text{U}$ and ${}^{240}\text{Pu}$ [1] (see Table II). Moreover, the $\langle \text{TKE} \rangle$'s and their dispersions σ_{TKE}^2 of the modes show a trend: $\langle \text{TKE} \rangle_{\text{S1}} > \langle \text{TKE} \rangle_{\text{S2}} > \langle \text{TKE} \rangle_{\text{SL}}$ and $\sigma_{\text{TKE,S1}}^2 < \sigma_{\text{TKE,S2}}^2 < \sigma_{\text{TKE,SL}}^2$, respectively. These trends agree with the findings of Refs. [54,55]. For the deformed nucleus at scission in the SL channel, the distance between the charge centers of the nascent fission fragments is greater than that for the S2 channel. Consequently, the average TKE of the SL channel is lower than that of the S2 channel ($\langle \text{TKE} \rangle_{\text{SL}} < \langle \text{TKE} \rangle_{\text{S2}}$) [1]. This is reflected in the $\langle \text{TKE} \rangle$ versus fragment mass plot. The $\langle \text{TKE} \rangle$ is minimum for symmetric and near-symmetric events [see Figs. 2(i)–2(l)].

C. Asymmetric to symmetric ratio

The ratio of the asymmetric-fission yield (Y_A) to the symmetric-fission yield (Y_S) versus excitation energy (E^*) according to the decompositions of MD and M-TKED of ${}^6\text{Li} + {}^{232}\text{Th}$ (in Figs. 4–7), is presented in Fig. 8. The ratios of $n + {}^{237}\text{Np}$ [57], ${}^4\text{He} + {}^{232}\text{Th}$ [58], ${}^{16}\text{O} + {}^{238}\text{U}$ [2,39], ${}^{18}\text{O} + {}^{238}\text{U}$ [59], and ${}^{18}\text{O} + {}^{208}\text{Pb}$ [60] are also presented for the sake of comparison. It can be seen that the slope of Y_A/Y_S of ${}^6\text{Li} + {}^{232}\text{Th}$ (slope ≈ -0.07) is similar to that of ${}^{18}\text{O} + {}^{208}\text{Pb}$ (slope ≈ -0.05). This nearly linear behavior of

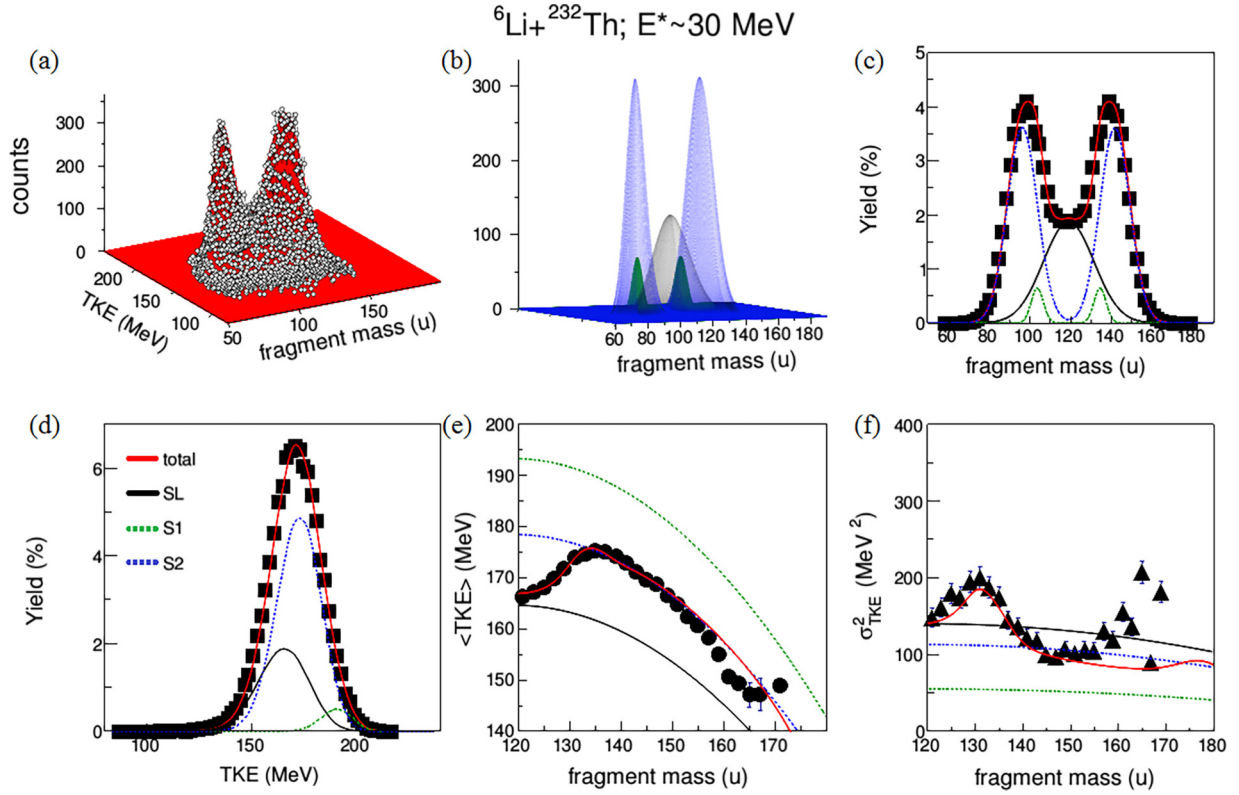


FIG. 4. (a) 2D fit to the M-TKEDs of ${}^6\text{Li} + {}^{232}\text{Th}$ at $E^* = 30 \text{ MeV}$. (b) The modes which constitute the 2D fit are shown, along with their projections to the (c) X axis (fragment mass) and (d) Y axis (TKE), and the mass dependence of (e) the $\langle \text{TKE} \rangle$ and (f) the σ_{TKE}^2 distributions. The continuous orange line represents the total fit. The continuous black, dashed green, and dashed blue represent the SL, S1, and S2 modes respectively, as shown in the legend in panel (d).

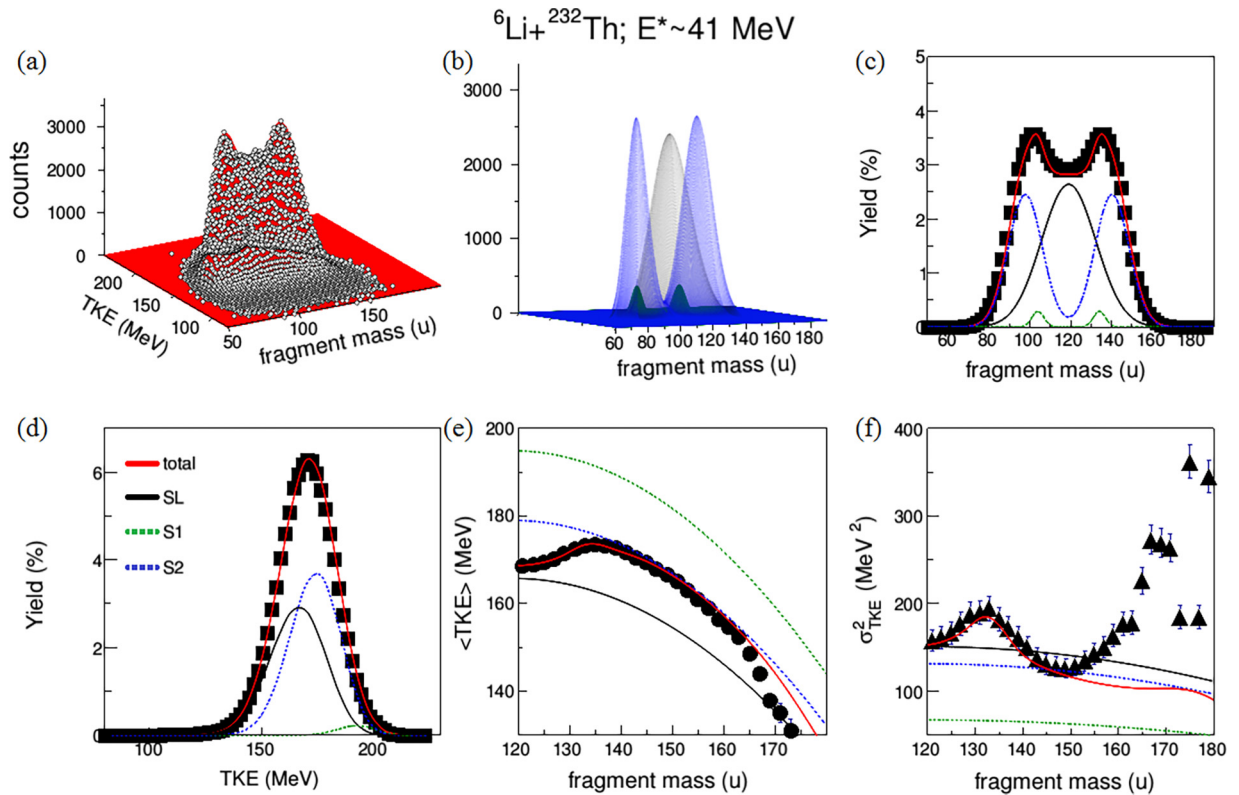


FIG. 5. Same as in Fig. 4 but at $E^* = 41 \text{ MeV}$.

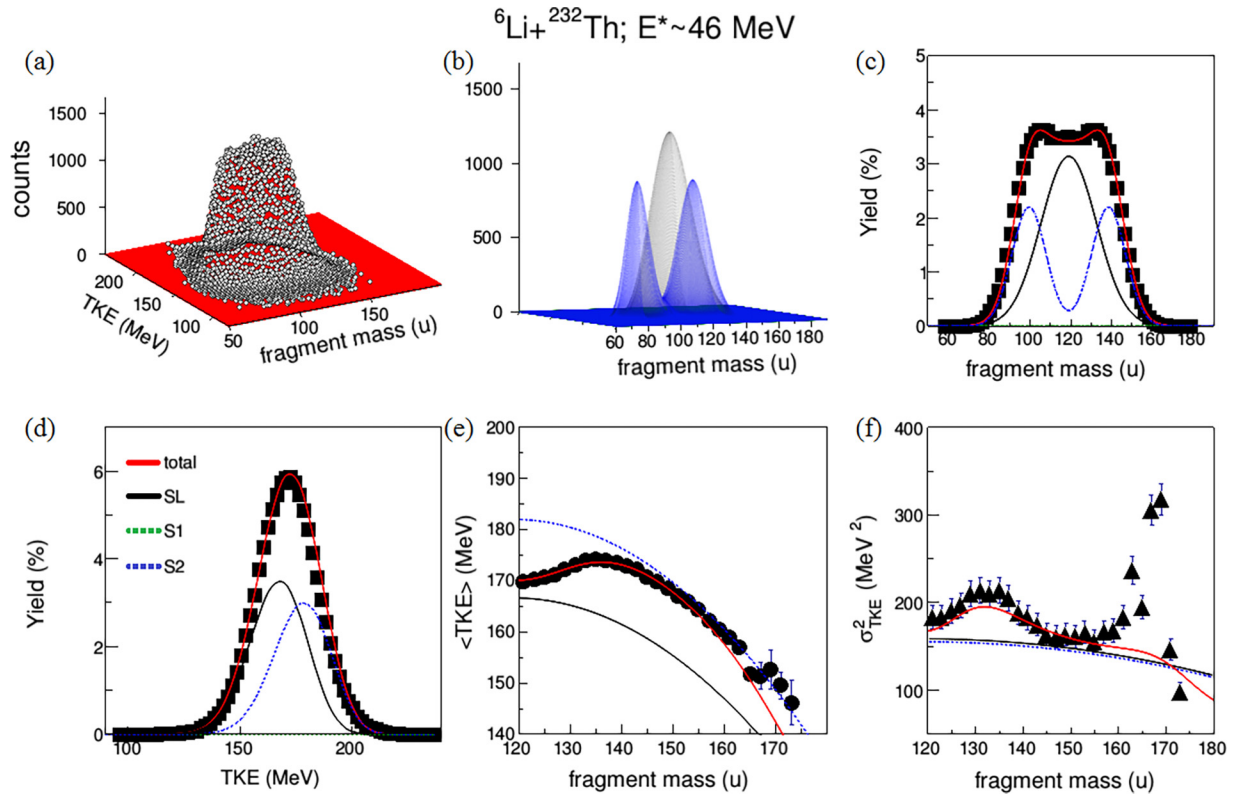


FIG. 6. Same as in Fig. 4 but at $E^* = 46 \text{ MeV}$.

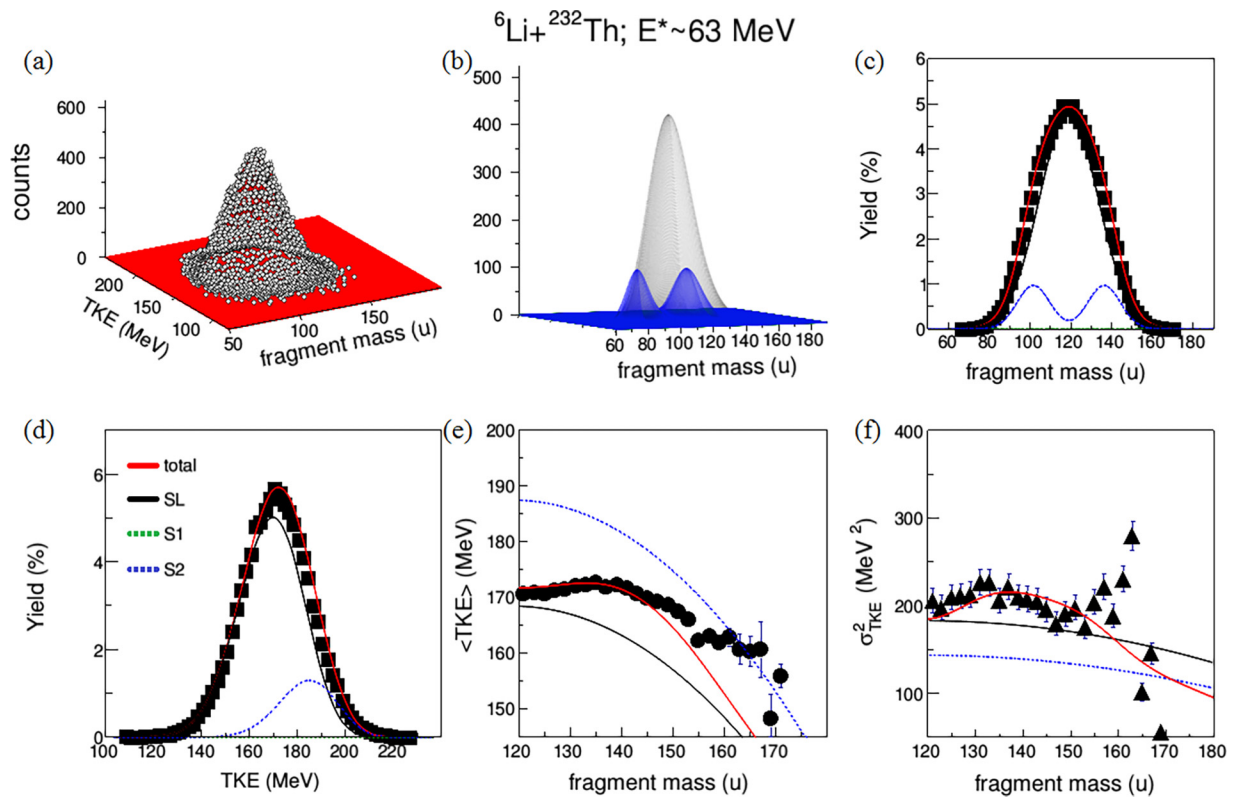


FIG. 7. Same as in Fig. 4 but at $E^* = 63 \text{ MeV}$.

TABLE II. Results of 2D fitting of the M-TKEDs of ${}^6\text{Li} + {}^{232}\text{Th}$ at four energies. Corresponding E^* 's of the CN are mentioned. Values labeled with † were kept fixed during the fitting. The reduced χ^2 ($\tilde{\chi}^2$) for each fit is mentioned. The average kinetic energy release in fission ($\langle\text{TKE}_{\text{fiss}}\rangle$) for this reaction obtained from Viola systematics ($\text{TKE}_{\text{Viola}}$) [28,56] and the prescription of Denisov *et al.* [63] are also mentioned. The $\langle M_H \rangle$ and $\langle\text{TKE}\rangle$ values of the fission modes of SF of ${}^{236}\text{U}$ and ${}^{240}\text{Pu}$ (from Ref. [1]) are also given in the last four columns for the sake of comparison.

E^* (MeV)	$\tilde{\chi}^2$	Modes	Y (%)	$\langle M_i \rangle$ (u)	σ_m (u)	$\langle\text{TKE}\rangle$ (MeV)	$\langle\text{TKE}_{\text{fiss}}\rangle$ (MeV)	σ_{TKE} (MeV)	$\langle M_H \rangle_{\text{SF}}^{236\text{U}}$ (u) [1]	$\langle M_H \rangle_{\text{SF}}^{240\text{Pu}}$ (u) [1]	$\langle\text{TKE}\rangle_{\text{SF}}^{236\text{U}}$ (MeV) [1]	$\langle\text{TKE}\rangle_{\text{SF}}^{240\text{Pu}}$ (MeV) [1]	
30	1.3	SL	28.9 ± 0.3	119.0^\dagger	12.31^\dagger	164.6 ± 0.20	171.7	11.8 ± 0.14					
		S1	4.80 ± 0.2	134.4 ± 0.11	3.0^\dagger	190.1 ± 0.30		7.4 ± 0.21					
		S2	66.3 ± 0.5	141.5 ± 0.07	7.3 ± 0.04	172.1 ± 0.11		10.4 ± 0.08					
41	2.9	SL	45.3 ± 0.1	119.0^\dagger	13.14^\dagger	165.8 ± 0.05	[28]	12.3 ± 0.03					
		S1	2.2 ± 0.03	134.0^\dagger	3.0^\dagger	191.8 ± 0.13	173.2 ± 3.04	8.2 ± 0.09					
		S2	52.5 ± 0.1	140.0^\dagger	8.3 ± 0.01	173.4 ± 0.04	[56]	11.3 ± 0.03	118.0	—	157.0	—	
46	2.8	SL	53.8 ± 0.1	119.0^\dagger	13.45^\dagger	166.6 ± 0.06	166.7	12.6 ± 0.05	134.0	134.0	187.0	192.0	
		S1	0.0^\dagger	—	—	—		—	—	141.0	140.0	167.0	175.0
		S2	46.2 ± 0.1	138.3 ± 0.02	8.3 ± 0.01	177.2 ± 0.07		[63]	12.3 ± 0.05				
63	2.5	SL	81.6 ± 0.2	119.0^\dagger	14.34^\dagger	168.5 ± 0.11	166.7	13.5 ± 0.08					
		S1	0.0^\dagger	—	—	—		—	—				
		S2	18.4 ± 0.2	136.2 ± 0.08	8.03 ± 0.06	183.57 ± 0.20			11.9 ± 0.14				

Y_A/Y_S in the measured energy range (on a logarithmic scale) indicates that the shell effects are damped exponentially with increasing excitation energy.

V. DISCUSSIONS AND CONCLUSIONS

The M-TKED of fission fragments of the reaction ${}^6\text{Li} + {}^{232}\text{Th}$ at excitation energies $E^* = 30, 41, 46,$ and 63 MeV have been analyzed with a 2D ansatz based on the multimodal random neck rupture model. The $\langle\text{TKE}\rangle$ is found to follow the same trend observed by Brosa *et al.* [1] in neighboring nuclei ${}^{236}\text{U}$ and ${}^{240}\text{Pu}$. The fission channel probabilities and the characteristics of different modes are obtained and

discussed in detail. It should be mentioned here that these probabilities may vary with the initial condition imposed during the fitting procedure but with no or little change in the mean mass and TKE of different fission modes.

The average kinetic energy release in fission obtained from the Viola systematic ($\text{TKE}_{\text{Viola}} = 173.2 \pm 3.04$ MeV [56]) matches with that of the Standard 2 mode $\langle\text{TKE}\rangle_{\text{S2}}$ (≈ 176.6 MeV). This is in agreement with the findings of Refs. [2,61,62]. $\text{TKE}_{\text{Viola}}$ does not match with the $\langle\text{TKE}\rangle$ of the broad symmetric SL mode (≈ 166.4 MeV). But, the most probable kinetic energy obtained from the prescription of Denisov *et al.* [63] (≈ 166.7 MeV) matches well with the value obtained in the present analysis for the SL mode. It should be noted here that in the systematic of Viola no dependence on the excitation energy of the fissioning nucleus is taken into account. At the ground state the S2 channel overpowers the SL channel. With increasing excitation the contribution from SL increases, and asymmetric fission decreases with the fading out of shell effects. Thus the total kinetic energy associated with asymmetric fission decreases with increasing excitation [2,51,63–67].

The 2D fitting method allows one to highlight the correlation between the fission modes in mass space with the fission mode in TKE space. The most important result of this application is summarized in Fig. 9. At every excitation energy, we notice that there is a transition from the S2 mode (more compact) to SL mode (more deformed) when fission becomes more asymmetric. In other words, in order for the nucleus to fission symmetrically, the fission point shape must be more deformed than in the case of asymmetric fission. This is an interesting clue that is substantially independent of the method used for fitting and possible biases due to the initial conditions. With increasing deformation at scission, the distance between the charge centers of the nascent fission fragments increases, which consequently provokes the decrease of the associated $\langle\text{TKE}\rangle$. The two-dimensional fit

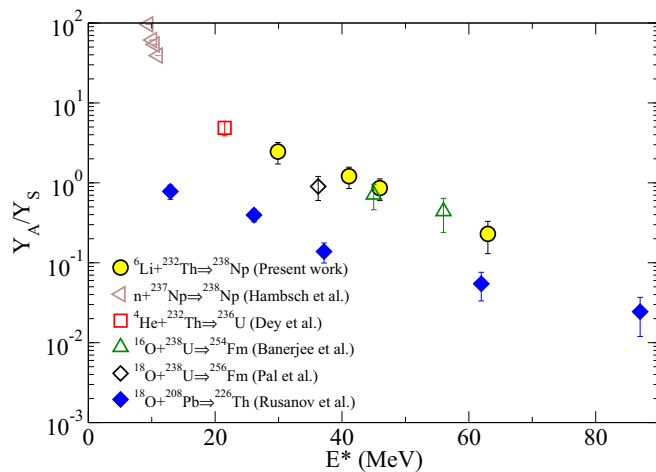


FIG. 8. Ratio of the asymmetric-fission yield (Y_A) to the symmetric-fission yield (Y_S) versus excitation energy (E^*) according to the decompositions of 2D M-TKED of ${}^6\text{Li} + {}^{232}\text{Th}$ in Figs. 4–7. The ratios of $n + {}^{237}\text{Np}$ [57], ${}^4\text{He} + {}^{232}\text{Th}$ [58], ${}^{16}\text{O} + {}^{238}\text{U}$ [2,39], ${}^{18}\text{O} + {}^{238}\text{U}$ [59], and ${}^{18}\text{O} + {}^{208}\text{Pb}$ [60] are also presented.

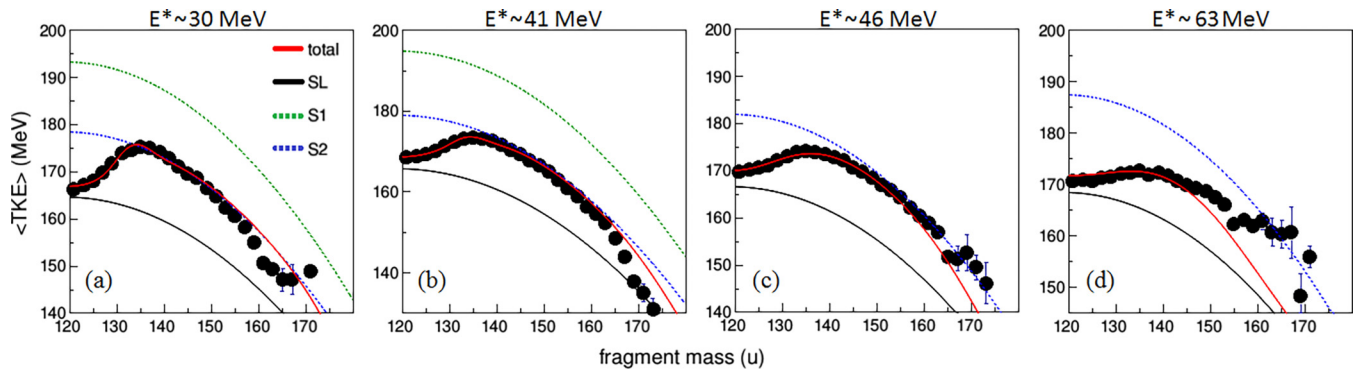


FIG. 9. $\langle TKE \rangle$'s against the mass of the binary fragments of the reaction ${}^6\text{Li} + {}^{232}\text{Th}$ at $E^* = 30, 41, 46,$ and 63 MeV are shown in panels (a)–(d). The color scheme for different fission modes is same as in Fig. 4–7 and is shown in the legend in panel (a).

highlights the dependence of TKE on mass and deformation of the fragments at the scission point. From Fig. 9 (which is a compilation of the $\langle TKE \rangle$ versus fragment mass plots from Figs. 4–7), it can be seen that in the symmetric mass region (≈ 120) $\langle TKE \rangle_{\text{SL}}$ is the one which is contributing most to the total $\langle TKE \rangle$. In other words, SL is the most probable mode for fission in the symmetric region. There is no presence of SS mode in this reaction. From the fragment mass ≈ 140 , S2 becomes the most probable mode for fission. There is a gradual transition from lower $\langle TKE \rangle$ at fragment mass ≈ 120 to higher $\langle TKE \rangle$ at mass ≈ 140 . As mentioned earlier, the component required other than the SL mode to fit the M-TKED in the case of last two high energies may represent a superposition of the multiple asymmetric modes (S1, S2, etc.), leading to an increase in the $\langle TKE \rangle$.

The slope of asymmetric to symmetric fission yields (when plotted against E^*) of ${}^6\text{Li} + {}^{232}\text{Th}$ in the measured energy range (slope ≈ -0.07) is found to be similar to that of previously reported ${}^{18}\text{O} + {}^{208}\text{Pb}$ (slope ≈ -0.05). This proves the absence of asymmetric quasifission in ${}^6\text{Li} + {}^{232}\text{Th}$.

Assuming unchanged charge density, the heavy fragments of S1 and S2 modes are found to peak at $Z \approx 52$ and $Z \approx 55$, respectively, in this work. This is in agreement with the finding of Böckstiegel *et al.* [68], where the authors found those values stable at $Z \approx 53$ and $Z \approx 55$, respectively, after systematically investigating the characteristics of multimodal fission of 15 nuclei around ${}^{226}\text{Th}$. The measurement of the atomic number of the fission fragments would aid in deeper understanding.

ACKNOWLEDGMENTS

The authors thank the FLNR accelerator team for their invaluable assistance during the experiment. The support of the directorate of the FLNR, JINR is greatly acknowledged. One of the authors (T.B.) acknowledges support from FLNR (Dubna) and INFN (Napoli) and is thankful to Dr. Ali Al-Adili, Dr. Alf Göök, and Dr. Chiranjib Mondal for fruitful discussions.

- [1] U. Brosa, S. Grossmann, and A. Müller, *Phys. Rep.* **197**, 167 (1990).
- [2] T. Banerjee, E. M. Kozulin, N. T. Burtebayev, K. B. Gikal, G. N. Knyazheva, I. M. Itkis, K. V. Novikov, T. N. Kvochkina, Y. S. Mukhamejanov, and A. N. Pan, *Phys. Rev. C* **105**, 044614 (2022).
- [3] D. R. Zolnowski, H. Yamada, S. E. Cala, A. C. Kahler, and T. T. Sugihara, *Phys. Rev. Lett.* **41**, 92 (1978).
- [4] K. Siwek-Wilczyńska, E. H. du Marchie van Voorthuysen, J. van Popta, R. H. Siemssen, and J. Wilczyński, *Phys. Rev. Lett.* **42**, 1599 (1979).
- [5] M. Dasgupta, D. J. Hinde, R. D. Butt, R. M. Anjos, A. C. Berriman, N. Carlin, P. R. S. Gomes, C. R. Morton, J. O. Newton, A. S. Toledo, and K. Hagino, *Phys. Rev. Lett.* **82**, 1395 (1999).
- [6] J. Rangel, M. R. Cortes, J. Lubian, and L. F. Canto, *Phys. Lett. B* **803**, 135337 (2020).
- [7] H. Freiesleben, H. C. Britt, and J. Birkelund, and J. R. Huizenga, *Phys. Rev. C* **10**, 245 (1974).
- [8] J. R. Leigh, R. M. Diamond, A. Johnston, and J. O. Newton, and S. H. Sie, *Phys. Rev. Lett.* **42**, 153 (1979).
- [9] V. Jha, V. V. Parkar, and S. Kailas, *Phys. Rep.* **845**, 1 (2020).
- [10] T. K. Lim, *Phys. Lett. B* **47**, 397 (1973).
- [11] P. G. Roos III, D. A. Goldberg, N. S. Chant, R. Woody III, and W. Reichart, *Nucl. Phys. A* **257**, 317 (1976).
- [12] V. I. Kukulín, V. M. Krasnopoľsky, V. T. Voronchev, and P. B. Sazonov, *Nucl. Phys. A* **417**, 128 (1984).
- [13] C. Signorini, A. Edifizi, M. Mazzocco, M. Lunardon, D. Fabris, A. Vitturi, P. Scopel, F. Soramel, L. Stroe, G. Prete, E. Fioretto, M. Cinausero, M. Trotta, A. Brondi, G. La Rana, R. Moro, E. Vardaci, A. Ordine, G. Inghima, M. La Commara, D. Pierroutsakou, M. Romoli, M. Sandoli, A. Diaz-Torres, I. J. Thompson, and Z. H. Liu, *Phys. Rev. C* **67**, 044607 (2003).
- [14] E. Vardaci, P. K. Rath, M. Mazzocco, A. Di Nitto, G. La Rana, C. Parascandolo, D. Pierroutsakou, M. Romoli, A. Boiano, A. Vanzanella, M. Cinausero, G. Prete, N. Gelli, F. Lucarelli, C. Mazzocchi, M. La Commara, L. Fortunato, A. Guglielmetti, F. Soramel, L. Stroe, and C. Signorini, *Eur. Phys. J. A* **57**, 95 (2021).
- [15] I. M. Itkis, A. A. Bogachev, A. Yu. Chizhov, D. M. Gorodisskiy, M. G. Itkis, G. N. Knyazheva, N. A. Kondratiev, E. M. Kozulin,

- L. Krupa, S. I. Mulgin, I. V. Pokrovsky, E. V. Prokhorova, A. Ya. Rusanov, V. M. Voskressenski, and S. V. Zhdanov, *Phys. Lett. B* **640**, 23 (2006).
- [16] R. Raabe, C. Angulo, J. L. Charvet, C. Jouanne, L. Nalpas, P. Figuera, D. Pierroutsakou, M. Romoli, and J. L. Sida, *Phys. Rev. C* **74**, 044606 (2006).
- [17] L. F. Canto, P. R. S. Gomes, R. Donangelo, and M. S. Hussein, *Phys. Rep.* **424**, 1 (2006).
- [18] D. H. Luong, M. Dasgupta, D. J. Hinde, R. du Rietz, R. Rafiei, C. J. Lin, M. Evers, and A. Diaz-Torres, *Phys. Lett. B* **695**, 105 (2011).
- [19] P. K. Rath, M. Ashaduzzaman, E. Vardaci, A. Di Nitto, G. La. Rana, F. Davide, A. Pulcini, D. Quero, M. Mazzocco, D. Pierroutsakou, M. Cinausero, G. Prete, M. La Commara, C. Parascandolo, M. Romoli, and N. Gelli, *J. Phys.: Conf. Ser.* **863**, 012030 (2017).
- [20] K. J. Cook, E. C. Simpson, L. T. Bezzina, M. Dasgupta, D. J. Hinde, K. Banerjee, A. C. Berriman, and C. Sengupta, *Phys. Rev. Lett.* **122**, 102501 (2019).
- [21] A. Pal, S. Santra, D. Chattopadhyay, A. Kundu, A. Jhingan, P. Sugathan, B. K. Nayak, A. Saxena, and S. Kailas, *Phys. Rev. C* **99**, 024620 (2019).
- [22] T. Banerjee, D. J. Hinde, D. Y. Jeung, K. Banerjee, M. Dasgupta, A. C. Berriman, L. T. Bezzina, H. M. Albers, Ch. E. Düllmann, J. Khuyagbaatar, B. Kindler, B. Lommel, E. C. Simpson, C. Sengupta, B. M. A. Swinton-Bland, T. Tanaka, A. Yakushev, K. Eberhardt, C. Mokry, J. Runke, P. Thörle-Pospiech, and N. Trautmann, *Phys. Rev. C* **102**, 024603 (2020).
- [23] D. Paul, A. Sen, T. K. Ghosh, M. M. Shaikh, K. Atreya, Rajkumar Santra, Samir Kundu, T. K. Rana, K. Banerjee, C. Bhattacharya, S. Bhattacharya, J. K. Meena, D. C. Biswas, B. N. Joshi, N. Kumar, G. K. Prajapati, Y. K. Gupta, K. Mahata, K. Ramachandran, and S. Pal, *Phys. Rev. C* **104**, 024604 (2021).
- [24] E. M. Kozulin, A. A. Bogachev, M. G. Itkis, I. M. Itkis, G. N. Knyazheva, N. A. Kondratiev, L. Krupa, I. V. Pokrovsky, and E. V. Prokhorova, *Instrum. Exp. Tech.* **51**, 44 (2008).
- [25] W. J. Nicholson and I. Halpern, *Phys. Rev.* **116**, 175 (1959).
- [26] B. B. Back, K. L. Wolf, A. C. Mignerey, C. K. Gelbke, T. C. Awes, H. Breuer, V. E. Viola, Jr., and P. Dyer, *Phys. Rev. C* **22**, 1927 (1980).
- [27] V. E. Viola, B. B. Back, K. L. Wolf, T. C. Awes, C. K. Gelbke, and H. Breuer, *Phys. Rev. C* **26**, 178 (1982).
- [28] V. E. Viola, Jr., *Nucl. Data Sheets, Sect. A* **1**, 391 (1965).
- [29] R. Bass, *Nuclear Reactions with Heavy Ions* (Springer, New York, 1980), Chap. 7.4, pp. 318–340.
- [30] H. Freiesleben, G. T. Rizzo, and J. R. Huizenga, *Phys. Rev. C* **12**, 42 (1975).
- [31] J. R. Birkelund, J. R. Huizenga, H. Freiesleben, K. L. Wolf, J. P. Unik, and V. E. Viola, Jr., *Phys. Rev. C* **13**, 133 (1976).
- [32] A. J. Sierk, *Phys. Rev. C* **33**, 2039 (1986).
- [33] J. P. Blocki, H. Feldmeier, and W. J. Swiatecki, *Nucl. Phys. A* **459**, 145 (1986).
- [34] U. L. Businaro and S. Gallone, *Nuovo Cim.* **5**, 315 (1957).
- [35] A. A. Bogachev, E. M. Kozulin, G. N. Knyazheva, I. M. Itkis, M. G. Itkis, K. V. Novikov, D. Kumar, T. Banerjee, I. N. Diatlov, M. Cheralu, V. V. Kirakosyan, Y. S. Mukhamejanov, A. N. Pan, I. V. Pchelintsev, R. S. Tikhomirov, I. V. Vorobiev, M. Maiti, R. Prajapat, R. Kumar, G. Sarkar, W. H. Trzaska, A. N. Andreyev, I. M. Harca, and E. Vardaci, *Phys. Rev. C* **104**, 024623 (2021).
- [36] E. M. Kozulin, G. N. Knyazheva, I. M. Itkis, M. G. Itkis, Y. S. Mukhamejanov, A. A. Bogachev, K. V. Novikov, V. V. Kirakosyan, D. Kumar, T. Banerjee, M. Cheralu, M. Maiti, R. Prajapat, R. Kumar, G. Sarkar, W. H. Trzaska, A. N. Andreyev, I. M. Harca, A. Mitu, and E. Vardaci, *Phys. Rev. C* **105**, 014607 (2022).
- [37] M. G. Itkis and A. Ya. Rusanov, *Phys. Part. Nucl.* **29**, 160 (1998).
- [38] G. D. Adeev and V. V. Pashkevich, *Nucl. Phys. A* **502**, 405 (1989).
- [39] T. Banerjee, E. M. Kozulin, K. B. Gikal, I. M. Itkis, G. N. Knyazheva, N. I. Kozulina, K. V. Novikov, I. N. Diatlov, I. V. Pchelintsev, A. N. Pan, and I. V. Vorobiev, *Phys. Part. Nucl.* **53**, 135 (2022).
- [40] Y. W. Wu, Z. H. Liu, C. J. Lin, H. Q. Zhang, M. Ruan, F. Yang, Z. C. Li, M. Trotta, and K. Hagino, *Phys. Rev. C* **68**, 044605 (2003).
- [41] S. E. Vigdor, H. J. Karwowski, W. W. Jacobs, S. Kailas, P. P. Singh, F. Soga, and T. G. Throwe, *Phys. Rev. C* **26**, 1035 (1982).
- [42] K. Hagino, N. Rowley, and A. J. Kruppa, *Comput. Phys. Commun.* **123**, 143 (1999).
- [43] R. A. Broglia and A. Winther, *Heavy Ion Reactions* (Benjamin-Cummings, Reading, MA, 1981), Vol. 1.
- [44] M. K. Pradhan, A. Mukherjee, P. Basu, A. Goswami, R. Kshetri, S. Roy, P. Roy Chowdhury, M. Saha Sarkar, R. Palit, V. V. Parkar, S. Santra, and M. Ray, *Phys. Rev. C* **83**, 064606 (2011).
- [45] F. Plasil, D. S. Burnett, H. C. Britt, and S. G. Thompson, *Phys. Rev.* **142**, 696 (1966).
- [46] F. Plasil and H. W. Schmitt, *Phys. Rev. C* **5**, 528 (1972).
- [47] Z. Fraenkel, I. Mayk, J. P. Unik, A. J. Gorski, and W. D. Loveland, *Phys. Rev. C* **12**, 1809 (1975).
- [48] M. G. Itkis, V. N. Okolovich, A. Ya. Rusanov, and G. N. Smirenkin, *Z. Phys. A* **320**, 433 (1985).
- [49] J. P. Lestone, A. A. Sonzogni, M. P. Kelly, and R. Vandenbosch, *J. Phys. G: Nucl. Part. Phys.* **23**, 1349 (1997).
- [50] P. Siegler, F.-J. Hamsch, S. Oberstedt, and J. P. Theobald, *Nucl. Phys. A* **594**, 45 (1995).
- [51] A. Pica, A. T. Chemey, L. Yao, W. Loveland, H. Y. Lee, and S. A. Kuvin, *Phys. Rev. C* **102**, 064612 (2020).
- [52] U. Brosa, H.-H. Knitter, T.-S. Fan, J.-M. Hu, and S. L. Bao, *Phys. Rev. C* **59**, 767 (1999).
- [53] I. Tsekhanovich, H.-O. Denschlag, M. Davi, Z. Büyükmumcu, F. Gönnewein, S. Oberstedt, and H. R. Faust, *Nucl. Phys. A* **688**, 633 (2001).
- [54] S. D. Beizin, S. V. Zhdanov, M. G. Itkis, V. N. Okolovich, G. N. Smirenkin, and M. I. Subbotin, *Sov. J. Nucl. Phys.* **53**, 411 (1991).
- [55] S. I. Mulgin, V. N. Okolovich, and S. V. Zhdanova, *Phys. Lett. B* **462**, 29 (1999).
- [56] V. E. Viola, K. Kwiatkowski, and M. Walker, *Phys. Rev. C* **31**, 1550 (1985).
- [57] F.-J. Hamsch, F. Vivés, P. Siegler, and S. Oberstedt, *Nucl. Phys. A* **679**, 3 (2000).
- [58] A. Dey, D. C. Biswas, A. Chakraborty, S. Mukhopadhyay, A. K. Mondal, K. Mandal, B. Mukherjee, R. Chakrabarti, B. N. Joshi, L. A. Kinage, S. Chatterjee, S. Samanta, S. Das, Soumik Bhattacharya, R. Banik, S. Nandi, Shabir Dar, R. Raut, G. Mukherjee, S. Bhattacharyya, S. S. Ghugre, and A. Goswami, *Phys. Lett. B* **825**, 136848 (2022).

- [59] A. Pal, S. Santra, P. C. Rout, R. Gandhi, A. Baishya, T. Santhosh, R. Tripathi, and T. N. Nag, *Phys. Rev. C* **104**, L031602 (2021).
- [60] A. Y. Rusanov, M. G. Itkis, N. A. Kondratiev, V. V. Pashkevich, I. V. Pokrovsky, V. S. Salamatin, and G. G. Chubarian, *Phys. At. Nucl.* **71**, 956 (2008).
- [61] T. Ohsawa, *J. Nucl. Radiochem. Sci.* **3**, 93 (2002).
- [62] M. D. Usang, F. A. Ivanyuk, C. Ishizuka, and S. Chiba, *Sci. Rep.* **9**, 1525 (2019).
- [63] V. Y. Denisov and I. Yu. Sedykh, *Phys. Lett. B* **824**, 136814 (2022).
- [64] D. G. Madland, *Nucl. Phys. A* **772**, 113 (2006).
- [65] J. P. Lestone and T. T. Strother, *Nucl. Data Sheets* **118**, 208 (2014).
- [66] R. Yanez, J. King, J. S. Barrett, W. Loveland, N. Fotiades, and H. Y. Lee, *Nucl. Phys. A* **970**, 65 (2018).
- [67] T. Banerjee, E. M. Kozulin, G. N. Knyazheva, and I. M. Itkis, *Phys. At. Nucl.* **85**, 770 (2022).
- [68] C. Böckstiegel, S. Steinhäuser, K.-H. Schmidt, H.-G. Clerc, A. Grewe, A. Heinz, M. de Jong, A. R. Junghans, J. Müller, and B. Voss, *Nucl. Phys. A* **802**, 12 (2008).